ELSEVIER

Journal of Nuclear Materials 266–269 (1999) 175–181

journal of nuclear materials

Role of divertor geometry on detachment in ASDEX Upgrade

R. Schneider *, H.-S. Bosch, D. Coster, J.C. Fuchs, J. Gafert, G. Haas, A. Herrmann, M. Kaufmann, A. Kallenbach, J. Neuhauser, J. Schweinzer, U. Wenzel, ASDEX Upgrade Teams

Max-Planck-Institut für Plasmaphysik, EURATOM-IPP Association, Boltzmannstr.2, D-85748 Garching, Germany

Abstract

The change of the divertor plasma behaviour from Div-I to Div-II for ASDEX Upgrade as measured by a set of reconstructed or newly designed divertor diagnostics is presented. The Div-II configuration is characterised – due to the highly inclined target plates – by reflection of neutrals towards the separatrix. Therefore, detachment in Div-II starts rather early localised close to the separatrix. In contrast, the complete global divertor detachment is practically unchanged, because the outer parts of the SOL stay attached even for high densities. The power distribution on the divertor in Div-II is much broader than in Div-I, resulting in a large reduction of peak power loads both in L and H-mode (factor of 2–4) due to larger divertor radiation losses. The larger losses are caused by larger hydrogen losses, enhancement of carbon radiation due to radial transport and convective energy transport into the radiation zone and larger radial energy transport in the divertor. The new Div-II geometry shows larger neutral gas densities in the divertor for the same line averaged density and a much faster helium exhaust rate ($\tau^*_{He}/\tau_E \approx 4$) in H-mode. The neon compression is worse compared with helium. No strong effect on impurity compression and overall divertor performance was seen by puff and pump experiments, neither in Div-I nor in Div-II.

Keywords: ASDEX-Upgrade; B2/EIRENE; Detachment; Particle exhaust; Power loading

1. Introduction

One of the critical questions to be solved for ITER (or any other reactor) is the exhaust problem for power and particles consistent with good core confinement. The operational point for ITER even slightly above the Greenwald limit motivates the analysis of high density operation, especially for detached divertor conditions [1].

Optimised divertors have to be tested in existing machines based mainly on the idea of closing them very efficiently to the main chamber and, by the choice of the plate and baffle geometry, positively influencing the detachment properties and reducing the target power load especially close to the separatrix. Additionally, ASDEX Ugrade needed an improved divertor to be able to operate at increased heating power, especially with doubled NBI power of up to 20 MW for deuterium, without target power load problems leading e.g. to carbon blooms.

In this paper, we report on the effects of divertor geometry on detachment and core plasma performance in the poloidal divertor tokamak ASDEX Upgrade. Results with the original, relatively open (Div-I) divertor configuration are compared with those obtained with the new, fairly closed LYRA divertor (Div-II), being more similar to the present ITER reference design (Fig. 1).

Detached operation is favourable as an operational scenario to solve the peak power load problem by reducing the target power loads to values below 5 MW/m^2. In detached divertor operation one can identify essentially three loss mechanisms for reducing the target power load. The first, if one starts from the

* Corresponding author. Tel.: +49-89 329 901; fax: +49-89 3299 2200; e-mail: rfs@ipp.mpg.de.

0022-3115/99/$ – see front matter
PII: S0022-3115(98)00524-8

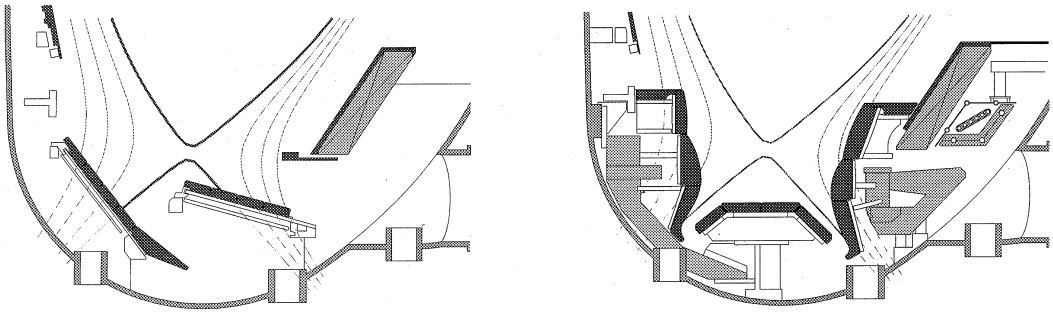

Fig. 1. Poloidal cross-section of ASDEX Upgrade with Div-I (left) and Div-II in the Lyra configuration (right).

target plate, is the loss through hydrogen, predominantly through radiation, which occurs at about 5–7 eV. The relatively low temperature also means that this loss channel gets only important if others have already reduced temperature and parallel power flow considerably compared to the midplane. The hydrogenic losses determine the detachment physics and – through the pressure balance profile along fieldlines – midplane scrape-off layer profiles and by this even core performance, e.g. through a scrape-off layer density limit. The charge exchange energy losses by hydrogen atoms are getting important only for the gas target cushion, removing the remaining small part of the parallel heat flux in front of the target and allowing onset of strong volume recombination [2]. The second loss mechanism is the loss through impurity radiation, which in the case of carbon as the dominant intrinsic impurity is occurring between 10–15 eV. These losses are very beneficial for the power load problem, because they do the necessary reduction of power flux and temperature to make the hydrogen losses important. A last mechanism can be the spreading of the power flow by radial transport. As we will see, it is also important in the analysis of the behaviour of the two divertor configurations in ASDEX Upgrade, especially for reduction of peak power loads even in attached operations.

2. Divertor configurations

The Div-I configuration (Fig. 1) was characterised by flat horizontal divertor plates, where the outer target plate was put close to the X-point to benefit from the large flux expansion in that region. The material was fine grain graphite. It had a relatively open divertor chamber with a small pumping baffle in the outer divertor, which nevertheless was quite important for good particle exhaust (see Section 5). For pumping, 14 turbomolecular pumps, adjacent to the outer divertor plate provided 12 m^3/s total pumping efficiency.

The new, fairly closed Div-II (Fig. 1) has curved vertical plates and is relatively deep and well baffled towards the main chamber. To maximise power exhaust capability even for attached conditions, CFC is used at the strike points. The pumping is done through the private flux region, where a dome baffle is used to enhance pumping. In addition to the turbomolecular pumps a cryopump has been installed with a pumping efficiency of 100 m^3/s.

3. Detachment properties

The old Div-I had a practically orthogonal inner plate and an outward tilted outer plate, reflecting the neutrals away from the hot zone close to the separatrix into the outer scrape-off layer. In contrast, the rationale for the construction of the Div-II configuration was the optimisation of neutral losses in the region close to the separatrix by strongly tilting the plate to reflect the neutrals preferentially into this hot region. This causes quite different detachment properties. In Div-I detachment as defined by a drop of the total ion saturation current by at least one order of magnitude developed rather uniformly and rather close to the density limit. In Div-II one observes an earlier detachment at the separatrix associated with an earlier onset of strong volume recombination (Fig. 2). This is accompanied by an earlier drop of the separatrix ion saturation current compared with Div-I as predicted by B2-Eirene modelling (Fig. 3). This reduction of detachment threshold with geometry was already seen on Alcator C-Mod [3] and in the new JET MK-II divertor [4].

Detachment in Div-II progresses from the separatrix to the outer scrape-off layer, which stays attached up to the global density limit. This effect also shows up in the B2-Eirene simulations. From these calculations, one also understands the observation that the earlier drop of the separatrix ion saturation current in Div-II is not seen in the total integrated particle flux, because in Div-II the outer scrape-off layer stays attached due to

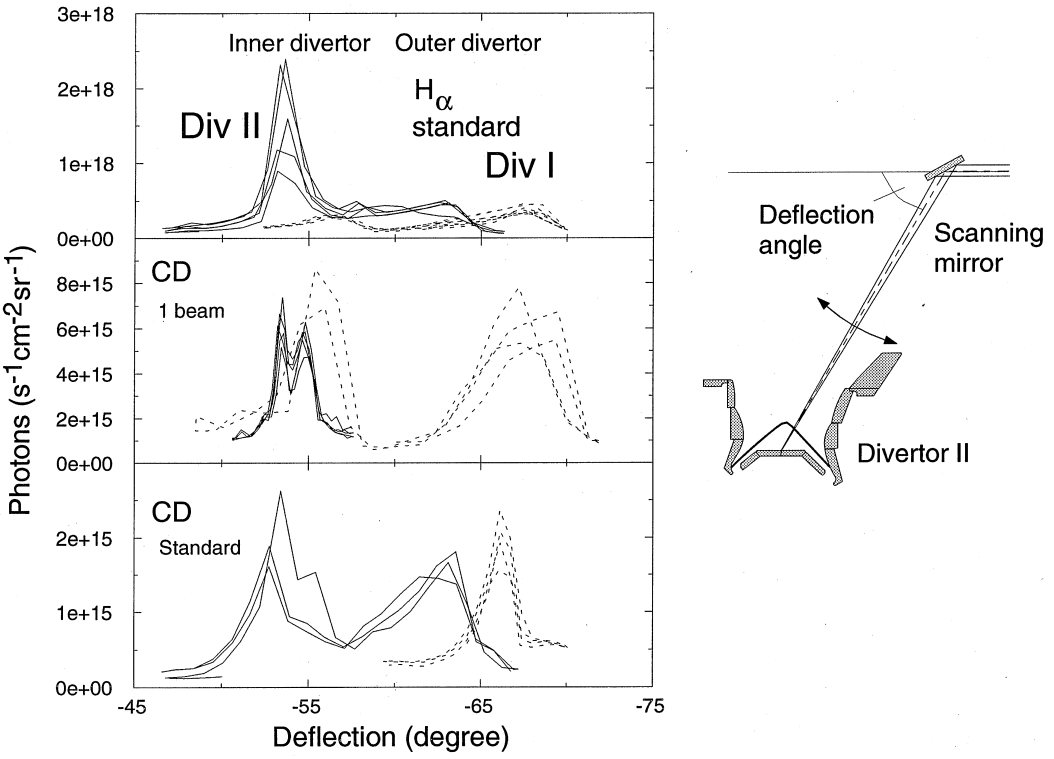

Fig. 2. Spectroscopic measurements (left) of H_α (top) as a function of deflection angle. The results are shown for both Div-I and Div-II for standard ohmic shot conditions and same line integral density range. Different curves represent different scans in time, respectively for different line integral densities. The location of the inner and the outer divertor are indicated in the top part of the figure. For Div-II the deepest part of the outer divertor is hidden by the divertor modules (see right part of the figure). For line integral densities, where one observes for Div-II a strong H_α emission in the inner divertor a much lower and more uniform H_α distribution is seen for Div-I. The strong H_α emission is a kind of fingerprint for the onset of strong volume recombination, existing at this range of line integral densities already in the inner divertor of Div-II, but not for Div-I. The spectroscopic measurements of CD band emission for same standard ohmic shot (bottom) and NBI heated shot conditions(middle) show no large difference for both divertor configurations. For some measurements the scan was not done for the whole divertor. On the right side the schematic setup of the spectroscopic line-of sights is shown.

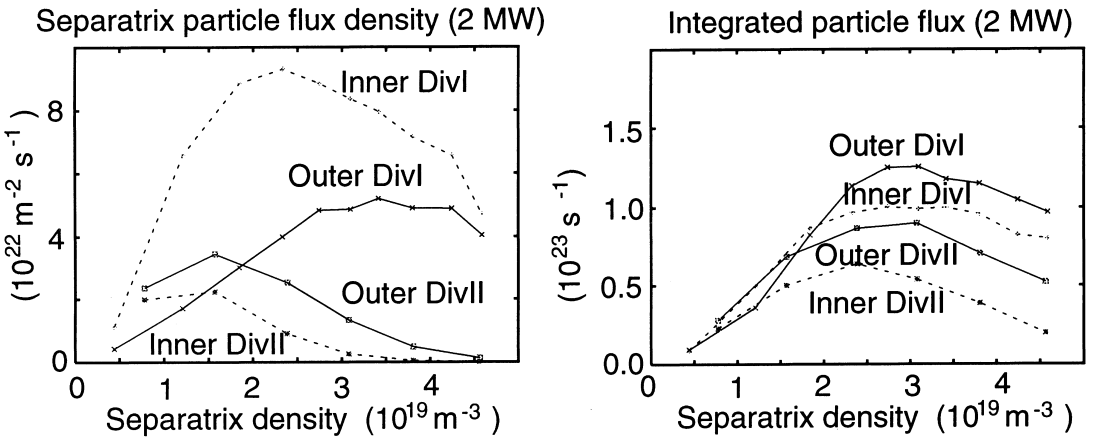

Fig. 3. B2-Eirene density-scan for pure hydrogen plasmas with 2 MW input power. On the left side, the dependence of the separatrix particle flux density is shown as a function of midplane separatrix density for inner and outer target in Div-I and Div-II. On the right side, the same dependence is plotted for the integrated particle flux.

inverted temperature profiles up to a global detachment of the target plates. This defines, for Div-II, an optimum operational window with a factor of 2 difference for upstream separatrix densities between start of detachment at the separatrix and complete global detachment, associated with the appearance of a MARFE on closed field lines and with the global L-mode density limit. This makes plausible, why the global density limits for Div-I and Div-II are the same, both in L and H-mode.

Specific detachment studies are possible in Div-II due to new diagnostics installed there. A detailed study of the recombining state was possible. This recombining phase is determined by the formation of a recombination ionisation double layer, where in the net recombining zone close to the target plates the plasma gets neutralised forming a kind of virtual target below a temperature of about 1 eV as measured by spectroscopy [5]. These neutrals then travel upstream in a 2-D way by leaving the zone sidewards and getting through multiple reflections at the side walls and the plasma into a hotter upstream regions where they are ionised (5–7 eV) [2]. In this ionisation front zone one drives quite large Mach flows even up to or above Mach equal 1 measured with a fast moveable Langmuir divertor probe [6] due to the large neutral sources there. In contrast, the net recombination zone is characterised by quite small flow velocities, as measured with a sophisticated toroidally viewing spectroscopy system [7], giving the plasma enough time to recombine.

4. Divertor power load

The power distribution on the divertor in Div-II is much broader than in Div-I, resulting in a large reduction of peak power loads both in L and H-mode (factor of 2–4) and now allowing a safe operation with less than 4 MW/m^2 in the full operational range without problems for the target plates even with 20 MW input power in H-mode [8]. This very positive effect is more than expected from simple geometry, because the outer target plate of Div-I had the same geometrical reduction due to field line inclination as the outer target plate of Div-II. The first did benefit from the large flux expansion close to the X-point, whereas the Div-II achieves the same by tilting the plate. Comparing the total power reaching the outer target as a function of the total heating power minus the radiation loss in the main chamber above the X-point (Fig. 4), it is obvious that the radiation losses in the divertor of Div-II are much larger than in the Div-I (by the factor of 2–4).

Comparing the bolometer deconvolution of radiation for two similar shots, the radiation pattern in Div-II is much more concentrated in the divertor with a pronounced maximum in the divertor tip and an emission

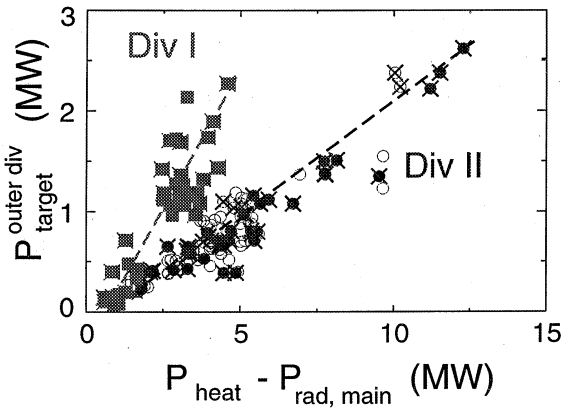

Fig. 4. The total power reaching the outer target plate $P_{\text{target}}^{\text{outerdiv}}$ as measured with thermography is shown as a function of the power going into the divertor, which is the difference of heating power P_{heat} and main chamber radiation $P_{\text{rad,main}}$ as determined from bolometry. Open symbols are hydrogen, full symbols deuterium shots. Crosses indicate H-mode conditions.

zone of carbon close to the separatrix, resulting in a larger divertor radiation for Div-II.

For the reduced power load, the different possible loss mechanisms have to be discussed. For relatively low power cases (total input power below about 2 MW), the effect of the preferential reflection of neutrals towards the separatrix with maximised losses can already explain for pure plasma conditions a factor of 2 reduction at high densities.

However, the experimental results of thermography, calorimetry and Langmuir measurements show this power load reduction also for attached conditions. That this effect has to be related to changes of the radial transport (or changes of the radial flow pattern) in the divertor region and not to changes of the upstream transport is experimentally indicated by no significant change of the midplane energy fall-off length from Div-I to Div-II [9].

In the code predictions the larger compression of the flux surfaces in the deeper divertor II results in larger anomalous radial fluxes when they are assumed to be described as a diffusion process determined by the local gradient in real space. This already produces for attached conditions a considerable broadening of the profile and by this a reduction of the power load maximum. If the diffusion process is assumed to be constant in flux-coordinates, this effect disappears.

Comparing the spectroscopically measured impurity production, e.g. by measurements of the CD bands (Fig. 2), for Div-I and Div-II the larger divertor radiation in Div-II cannot be understood by larger impurity production. The large values for the radiation losses of up to 10–20 MW/m^3 in Div-II can be explained by both the radial transport, allowing to enhance the radiation

volume [10] and the transport of energy into the radiation zone not only by conduction but predominantly by convection in the cold divertor region as already discussed by DIII-D [11].

The early onset of volume recombination in Div-II close to the separatrix also enhances the carbon losses there. Due to the slowing down of the parallel flow in this region, one gets a higher density of deuterium or hydrogen there. Also, the carbon residence time in the region near the separatrix is large, because the carbon ion mass flow pattern (Fig. 5) shows a flow reversal zone due to the ion thermal force with small flow velocities close to the separatrix and a forward flow in the outer scrape-off layer with relatively fast flow [7].

Spectroscopically determined radiation potentials for the dominant divertor radiator CIII, defined as the ratio of the radiation power emitted from the CIII charge state along a line-of sight and the influx of CIII along this line-of sight getting ionised, are strongly temperature dependent as shown in Fig. 6 using the ADAS database [12]. They reach values up to 2–3 keV for temperatures close to 10 eV, rather independent of electron density. This method is only applicable if the CIII has enough time to ionise, which means that one really measures spectroscopically a particle flux. Therefore, for lower temperatures the transport time has to get large to allow for this ionisation process. This is possible due to the reduced carbon ion flow in the radiation zone close to the separatrix. However, in regions close to the target plate with strong forward flow, the basic assumption for a flux measurement fails.

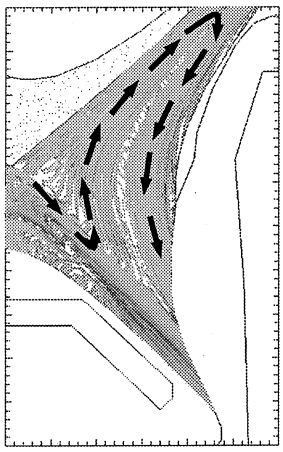

Fig. 5. The ion mass flow pattern for a B2-Eirene simulation with hydrogen and physically and chemically sputtered carbon for 4 MW input power and a midplane separatrix density of 2.6×10^{19} m^{-3}. Trace particles are started according to the distribution of the total carbon density in the outer divertor and followed according to the radial and parallel velocities until they reach either a B2 side-wall or the target plate. The total carbon velocities and densities are obtained from the sum of the individual transported carbon charge states. The flow pattern is characterised by a flow reversal zone close to the separatrix and a forward flow zone in the outer scrape-off layer. For guiding the eye the black arrows show one possible carbon trajectory.

B2-Eirene can be used to extract total radiation potentials for carbon defined as the ratio of total radiation loss by carbon to the carbon source flux rising with upstream density up to 2000 eV for cold divertor conditions showing the same trend as the experimental procedure.

The flow pattern is also quite important for the analysis of the exhaust properties, which will be done in Section 5.

All effects discussed before increase the losses in Div-II also in ELMy H-mode (Fig. 4) and broaden the deposition profile in the divertor like in L-mode. Therefore, one obtains in Div-II much lower peak power loads also during ELMs [8]. For type III ELMs one can get in Div-II detachment during ELMs like in the CDH mode in Div-I now even without adding extrinsic impurities. The same power and particle fluxes should enter during ELMs, the divertor in Div-II as in Div-I, because the limiting structure for the ELMs is still the contour of the 4 ICRH antennas, which follow typically the 3 cm midplane magnetic flux contour (see Section 5). Therefore, the narrow divertor entrance in Div-II does not affect the overall ELM characteristics. One difference exists due to the strongly inclined geometry in Div-II: the variation of the separatrix position during ELMs (several mm in the midplane) translate in Div-II into large shifts of the separatrix at the target plate (several cm distance along the target plate), whereas in Div-I for the more orthogonal plates no strong shift was observed.

5. Pumping and helium exhaust

As important as the power exhaust is the particle exhaust for any reactor, because removal of the helium ash is necessary to avoid extinguishing the burning plasma and good pumping is necessary to do burn control and feedback operations.

The design of Div-II was done for optimising the pumping capability by reducing the plasma pumping in the private flux region with a dome baffle [13]. As predicted by B2-Eirene one gets larger neutral gas flux densities in the divertor for the same midplane separatrix and line averaged densities [9,14]. In contrast, the main chamber neutral fluxes do not change [9,14] for medium and high densities, also consistent with B2-Eirene predictions. Therefore, the main chamber neutral flux is apparently not determined by the divertor leakage in Div-I or Div-II, but through main chamber recycling at baffles or limiters. The closest surfaces in the main chamber are 4 ICRH antennas, which follow typically the 3 cm midplane magnetic flux contour. Additionally,

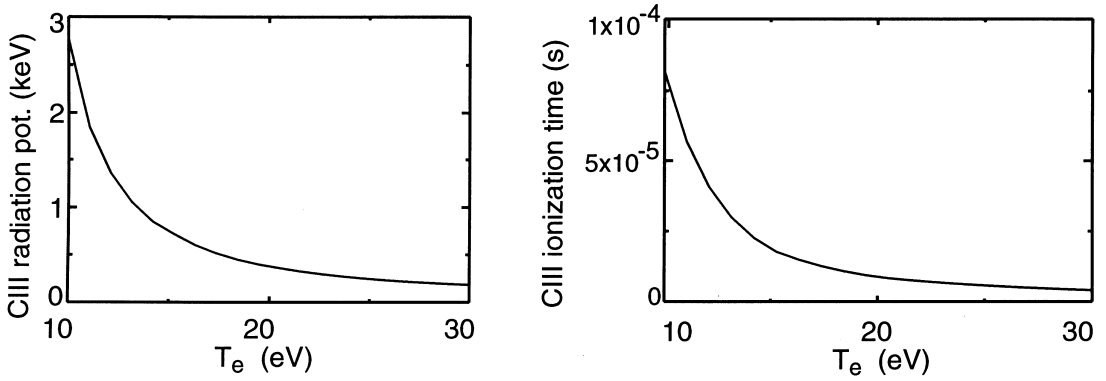

Fig. 6. CIII radiation potential as a function of temperature (left) from ADAS for an electron density of 1.0×10^{20} m^{-3}. CIII ionisation times as a function of temperature (right) from ADAS for an electron density of 1.0×10^{20} m^{-3}.

due to the existence of shoulders in density and temperature profiles (possibly caused by strongly enhanced turbulence by e.g. flute-like modes in the outer scrape-off layer [15]) extending even into the shadow of limiters one expects a contribution from direct main chamber recycling which is nearly independent of the distance of the closest limiting structure from the main plasma. Therefore, the closing of the divertor seems not to be too important for good core performance as long as the plasma plugging itself is doing well, which especially works very efficiently in the inclined target setup of Div-II with the attached outer scrape-off layer. From this argument, it is plausible that the core plasma performance, e.g. L- and H-mode density limits, confinement times and L–H threshold scaling, is practically unchanged from Div-I to Div-II. For low densities, which are usually not the standard ASDEX Upgrade operation, the main chamber neutral fluxes are reduced considerably [14], because for these conditions the divertor leakage is large and any improvement of the divertor baffling appear in the main chamber neutral fluxes.

The impurity (and also hydrogenic) compression in Div-I was determined by recycling in the outer scrape-off layer, where the existence of a small pumping baffle was quite important [16,17]. In contrast, in Div-II the feeding of the pump duct is now done through the private flux region. Experimentally, one observes in Div-II very good helium exhaust with $\tau^*_{He}/\tau_E \approx 4$ for H-mode conditions and, in contrast to Div-I, a much better compression of helium compared to neon [18,14]. Both measurements agree with B2-Eirene predictions, which allow an analysis of the different mechanisms. Due to the flow pattern of helium and neon which is rather similar to that of carbon one gets a second particle flux maximum away from the separatrix for impurities in both divertor configurations, in the region of the outer scrape-off layer with strong forward flow. In Div-II, neon and helium have to enter the pumping plenum by direct reflection of neutrals (neon and helium have no dominant charge–exchange process in contrast to hydrogen). Therefore, the longer mean free path of helium gives better compression for helium compared to neon [17].

Another check of this hypothesis is possible, because experiments where one vertically shifts the plasma varying by the intersection of the separatrix on the target plates show a strong sensitivity of helium and neon compression, whereas hydrogen compression and pumping is much less affected [14]. This is expected from the picture given before, because hydrogen compression and pumping is not determined by direct reflection of neutrals into the pumping plenum but through multiple CX collisions, whereas neon and helium compression are dominated by this ballistic effect.

In ASDEX Upgrade no strong effect on impurity compression and overall divertor performance was seen by puff and pump experiments, neither in Div-I nor in Div-II [14,19] in agreement with B2-Eirene predictions and in contradiction to results of DIII-D [20].

6. Conclusions

The change of the divertor plasma behaviour from Div-I to Div-II as measured by a set of reconstructed or newly designed divertor diagnostics seems to agree with modelling predictions by B2-Eirene.

The Div-II configuration is characterised – due to the highly inclined target plates – by reflection of neutrals towards the separatrix. Therefore, detachment in Div-II starts rather early, localised close to the separatrix. In contrast, the complete divertor detachment is practically unchanged, because the outer parts of the SOL stay attached even for high densities. This makes it plausible that Div-I and Div-II have the same global (line integral) density limits.

The power distribution on the divertor in Div-II is much broader than in Div-I, resulting in a large reduction of peak power loads both in L and H-mode (factor of 2–4) due to larger divertor radiation losses. The larger losses are caused by larger hydrogen losses, enhancement of carbon radiation due to radial transport and convective energy transport into the radiation zone and larger radial energy transport in the divertor.

The new Div-II geometry shows a stronger neutral gas scaling with line averaged density and a much faster helium exhaust rate ($\tau^*_{He}/\tau_E \approx 4$) in H-mode. The neon compression is worse compared with helium. All these effects can be understood from the different pump recycling through the dome baffle.

No strong effect on impurity compression and overall divertor performance was seen by puff and pump experiments, neither in Div-I nor in Div-II.

Over all, the Div-II results for ASDEX Upgrade demonstrate the possibility to optimise the geometry to obtain minimum power load together with optimum particle exhaust and large operational window without negatively affecting the core confinement. However, one loses experimental flexibility concerning MHD equilibria fitting into the divertor. Therefore, the design of a flexible divertor especially for high triangularity might need to relax some of the optimisation criteria.

References

[1] W. Suttrop et al., these Proceedings.
[2] K. Borrass et al., J. Nucl. Mater. 241–243 (1997) 250.
[3] B. Lipschultz et al., IAEA (1996) F1-CN-64/A4-5.
[4] R.D. Monk et al., ECA Part I (1997) 117–120.
[5] U. Wenzel et al., these Proceedings.
[6] N. Tsois et al., these Proceedings.
[7] J. Gafert et al., these Proceedings.
[8] A. Herrmann et al., these Proceedings.
[9] J. Schweinzer et al., these Proceedings.
[10] S. Krasheninikov et al., Contrib. Plasma Physics 36 (1996) 266ff.; 5th Workshop on Plasma Edge Theory, December 1995, Asilomar, USA.
[11] A.W. Leonard et al., Phys. Rev. Lett. 78 (1997) 4769.
[12] H.P. Summers, Atomic data and analysis structure, Technical Report Jet-IR(94)06, JET Joint Undertaking, Culham, 1994.
[13] R. Schneider et al., J. Nucl. Mater. 241–243 (1997) 701.
[14] H.-S. Bosch et al., these Proceedings.
[15] H.-S. Bosch et al., J. Nucl. Mater. 220–222 (1995) 558.
[16] D.P. Coster et al., J. Nucl. Mater. 241–243 (1997) 690.
[17] R. Schneider et al., in: Plasma Phys. and Cont. Nucl. Fusion Research 1996, vol. 2, International Atomic Energy Agency, Vienna, 1997, pp. 465–476.
[18] H.-S. Bosch et al., J. Nucl. Mater. 241–243 (1997) 82.
[19] H.-S. Bosch et al., Phys. Rev. Lett. 76 (1996) 2499.
[20] M.J. Schaffer et al., J. Nucl. Mater. 241–243 (1997) 585.